CrowdMagMap 2.0: Crowdsourced Magnetic Mapping for Multi-Floor Underground Parking Lot Navigation

Jian Kuang, Yan Wang, Longyang Ding, Baoding Zhou, *Member, IEEE*, Liping Xu, Li Cao, Lanqin He, Yunhui Wen, and Xiaoji Niu, *Member, IEEE*

***Abstract*—Location-based services (LBS) have become an integral part of daily life and work for the general public. However, achieving widespread and accurate positioning in typical indoor environments remains a significant challenge, particularly in multi-floor indoor parking lots where radio frequency signals like WiFi are often unavailable. Indoor magnetic matching presents a viable solution, but it requires reducing mapping costs through the use of crowdsourced data. To tackle this issue, we propose an innovative method for constructing magnetic maps using crowdsourced vehicle data. Our approach introduces a multi-user joint vehicle dead reckoning technique based on graph optimization, which provides consistent directional estimates of crowdsourced vehicle trajectories. Subsequently, we establish associations between different vehicle trajectories using multi-attribute features of the magnetic field. Building on this foundation, we propose a global trajectory optimization with inequality and equality constraints to achieve precise estimation of crowdsourced vehicle trajectories. Testing with simulated data from two three-floor underground parking lots demonstrates that the proposed method, utilizing only on-board smartphone sensor data, achieves plane and elevation errors of less than 2.75 meters (95%) and 0.59 meters (95%), respectively. Additionally, the magnetic matching positioning error based on crowdsourced magnetic sequence maps is less than 2.29 meters (95%).**

***Index Terms*—Crowdsource, magnetic map, keyframe association, vehicle navigation, indoor positioning.**

Received 21 December 2024; revised 22 May 2025; accepted 1 August 2025. This work was supported in part by the National Key Research and Development Program of China under Grant 2024YFB3909200, in part by the Open Research Fund Program of Geographical Environment Monitoring Key Laboratory for Geo-Environmental Monitoring of Great Bay Area, and in part by the China University Industry-University-Research Innovation Fund under Grant 2024HT008. The Associate Editor for this article was H. Jiang. *(Corresponding author: Yan Wang.)*

Jian Kuang, Yan Wang, Longyang Ding, and Xiaoji Niu are with the GNSS Research Center and the Hubei Technology Innovation Center for Spatiotemporal Information and Positioning Navigation, Wuhan University, Wuhan, Hubei 430072, China (e-mail: wystephen@whu.edu.cn).

Baoding Zhou is with the State Key Laboratory of Road Engineering in Extreme Environment and Institute of Urban Smart Transportation and Safety Maintenance, Shenzhen University, Shenzhen, Guangdong 518060, China.

Liping Xu, Li Cao, Lanqin He, and Yunhui Wen are with Shanghai Transsion Information Technology Ltd., Shanghai 201213, China.

Digital Object Identifier 10.1109/TITS.2025.3597273

I. Introduction

VEHICLE localization using smartphones is a vital component of consumer-grade positioning, forming the backbone of location-based services, big data applications, and the Internet of Things [1], [2]. While the widespread use of GNSS (Global Navigation Satellite System) enables smartphones to achieve meter-level positioning in outdoor open environments, which generally meets application requirements, there remains a lack of universally applicable methods for vehicle localization in typical indoor environment [3], [4], such as underground parking lots.

In indoor environments, smartphone localization methods encompass a variety of technologies, including Camera [5], [6], WiFi [7], [8], [9], Bluetooth Low Energy (BLE) [10], magnetic fields [11], [12], Ultra-Wideband (UWB) [13], [14], and Inertial Measurement Unit (IMU) [15], [16]. Among these, the IMU can only provide relative trajectories and is typically used as a foundation for integrating other positioning information to enhance overall accuracy [17], [18], [19]. UWB-based positioning has been improved by recent advancements in outlier detection [20], achieving decimeter-level precision in specific applications. However, its dependence on base station deployment and the lack of UWB reception in consumer devices limit its widespread applicability. Conversely, BLE-based positioning, augmented by deep learning techniques [21], [22] and particle swarm optimization [23], demonstrates high accuracy in certain environments. Although it utilizes existing smartphone hardware, this approach requires additional BLE base stations, which hinders its scalability as a universal positioning solution. WiFi-based positioning can achieve good accuracy in environments like shopping malls, but in settings such as indoor parking lots, WiFi base stations are often either absent or deployed too sparsely to provide reliable positioning. Vision-based and magnetic field-based positioning technologies rely solely on the building's infrastructure and can achieve very high accuracy.

Technologies like Vision and Magnetic Fields do not rely on infrastructure construction but do depend on pre-built signal fingerprint maps. To facilitate the widespread application of indoor positioning, the development of signal fingerprint maps using crowdsourced data has been proposed. Research into building signal fingerprint maps based on crowdsourced data

for Vision has already garnered significant attention. In indoor environments, the high measurement accuracy of Vision technology enables mapping and positioning to achieve meter-level precision [24], [25]. However, for mass consumer applications on smartphones, the computational complexity of visual positioning remains prohibitively high, posing challenges for its widespread adoption.

Due to their relatively lower computational demands, magnetic field-based methods have found some application in indoor positioning. However, research on constructing crowdsourced magnetic field maps has primarily focused on approaches utilizing pedestrian crowdsourced data. Luo et al. [26] and Ayanoglu et al. [27] address indoor office scenarios by modeling pedestrian trajectories as compositions of straight lines and corners. They correlate different trajectories based on these features to reconstruct user paths and magnetic field maps. Kwak et al. [28] enhances this approach by incorporating motion distance information, which helps reduce the computational burden associated with magnetic sequence matching using Dynamic Time Warping. CrowdMagMap [29] further advances these methods by relaxing assumptions about crowdsourced data. It addresses real-world challenges such as pedestrian free movement, random smartphone holding postures, and short trajectory lengths, and presents a method for reconstructing magnetic field maps of single-floor scenes using pedestrian crowdsourced data. However, for services such as indoor vehicle positioning and parking navigation, it is necessary to construct a magnetic field map of a multi-story indoor parking lot. The methods previously employed typically lack cross-floor data in the pedestrian crowdsourced data, which limits their ability to meet this requirement.

This paper focuses on how to construct magnetic field maps of multi-storey parking lots using passive crowdsourced data from smartphones and addresses the following two challenges: 1) The typical accuracy of smartphone built-in sensors is low, and there is a lack of widely available high-reliability absolute positioning methods in indoor scenarios, which makes it difficult to restore accurate, smooth and heading-correct vehicle trajectories. 2) The magnetic field map of a multi-storey parking lot requires the reconstruction of the three-dimensional shape of the vehicle trajectory, which is significantly different from the existing magnetic map construction task based on pedestrian crowdsourced data and is more complex. The main contributions of this work are summarized as follows:

- We propose a novel algorithm to generate magnetic field maps of indoor multi-storey parking lots using crowdsourced data from smartphones with embedded inertial measurement units (IMUs) and magnetometers. Based on a graph optimization algorithm framework, the proposed algorithm integrates IMU measurements, vehicle motion models, and magnetic field information without relying on prior knowledge of smartphone mounting angles, lever arm configurations, or magnetometer pre-calibration. To the best of our knowledge, this is the first method designed specifically for this challenging task.
- We propose an optimization algorithm that jointly estimates the global pose and performs floor clustering. Through multiple iterations of floor clustering and global trajectory optimization, the proposed method can accurately recover the global 3D magnetic field sequence map even in the presence of significant errors in vehicle elevation estimation in crowdsourced data.
- We validate the feasibility of the proposed algorithm using simulated crowdsourced data from two typical three-storey indoor parking lots and demonstrate that the crowdsourced magnetic field map can support meter-level vehicle indoor positioning.

The remainder of the paper is organized as follows. Section II gives an overview of the proposed method. Section III describes the multi-user joint vehicle dead reckoning. Section IV describes the global trajectory optimization method. Section V uses field tests to evaluate the proposed method.

II. System Overview

The concept of crowdsourced magnetic field mapping involves delegating the demanding task of data collection to everyday users. By analyzing the sensor readings from smartphones carried by these users, we can reconstruct indoor magnetic field maps, achieving this at a low cost. However, the challenge lies in the fact that sensor data are collected as users move naturally and dynamically, with their positions unknown, and the data from any single user is typically brief. Thus, the key to successful crowdsourced magnetic mapping is accurately determining users' actual movement trajectories and establishing spatial correlations between different users.

Figure 1 illustrates the algorithmic flow of the proposed method, which comprises three main components: Trajectory Estimation, Trajectory Association, and Global Trajectory Optimization. Trajectory Estimation utilizes smartphone sensor observations to estimate the motion trajectories of various vehicles, transforming these observations into spatial information. By leveraging the estimated vehicle trajectories and magnetic field features, Trajectory Association identifies spatial associations between different vehicle trajectories, pinpointing moments when different vehicles pass the same location. Global Trajectory Optimization integrates the estimated vehicle trajectories with the spatial association information to achieve a globally optimal estimation of the relative trajectories among all vehicles.

In Trajectory Estimation, a filter-based vehicle dead reckoning (VDR) method is employed to seamlessly integrate sensor observations with vehicle motion constraints in real time. This filter-based VDR is capable of adaptively detecting the vehicle's motion state and estimating the positional relationship between the smartphone and the vehicle, thereby providing a more precise initial value for trajectory estimation during data post-processing [30]. The multi-user joint VDR framework is built upon a graph optimization algorithm architecture. It effectively integrates incremental motion constraints and ensures global consistency by incorporating magnetic vector observations from different vehicles within the same spatial environment. This approach enhances the precision and reliability of vehicle trajectory estimates by leveraging data from multiple users.

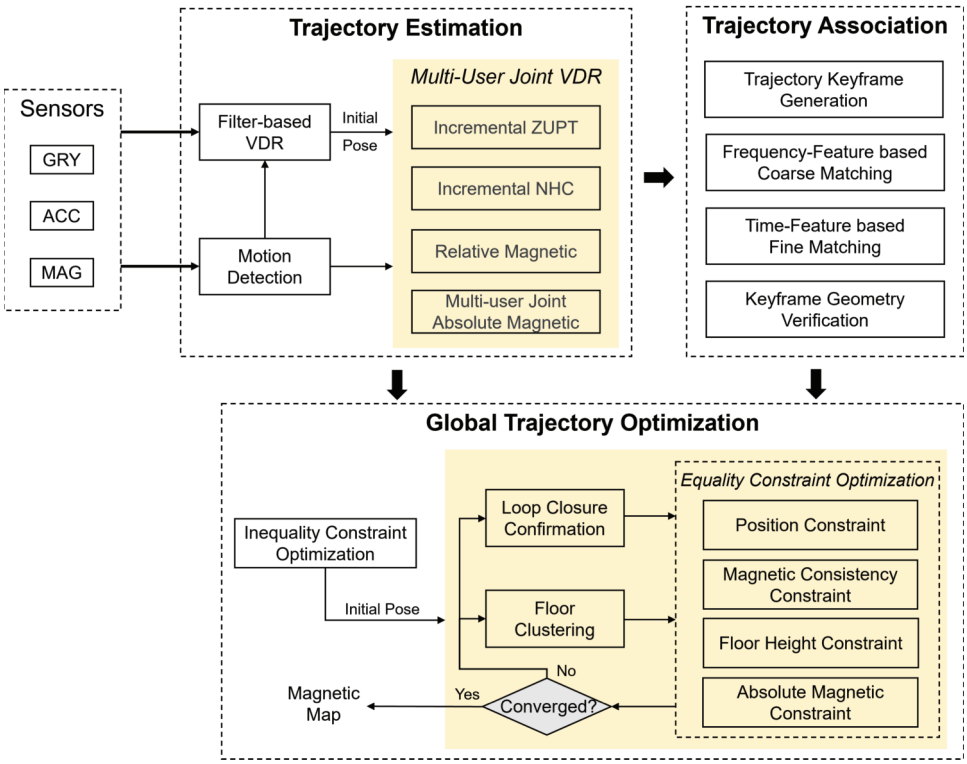

Fig. 1. System framework of the proposed crowdsourced magnetic field mapping method. The orange background part is the main contribution of this algorithm.

In the Trajectory Association, the vehicle trajectories are divided into segments (i.e. keyframes) of 20 meters in length. The observed magnetic features are then resampled based on spatial distance. Building on this foundation, magnetic features in the frequency domain are employed for the coarse matching of keyframe pairs, enhancing the efficiency of the trajectory association algorithm. Subsequently, magnetic features in the time domain are utilized for the fine matching of keyframe pairs. To ensure the accuracy of the trajectory association algorithm, the geometric similarity of keyframe pairs is used for verification. Further details of this algorithm are available in our published paper [29].

In the Global Trajectory Optimization, inequality constraint optimization leverages the relative pose and initial position and heading provided by VDR to represent a single trajectory. This approach significantly reduces the number of parameters that need optimization, thereby facilitating rapid screening and verification of associated keyframe pair information and ensuring both efficiency and reliability in solving constraint problems. Building on this, equality constraint optimization utilizes the original observations from the IMU to mitigate any accuracy loss that might occur from relying solely on the relative pose output by VDR. Through multiple iterations, this method defines the optimization problem to achieve global trajectory optimization.

In summary, the core algorithms of the proposed method are multi-user joint VDR and global trajectory optimization. These algorithms are crucial in assessing the feasibility of the method. Consequently, the subsequent sections of the paper will concentrate on these two algorithms, exploring their implementation, effectiveness, and role in the overall trajectory association and optimization framework.

III. Multi-User Joint Vehicle Dead Reckoning

In indoor environments, accurately estimating vehicle trajectories using only the smartphone's built-in IMU can be quite challenging without prior signal base stations and positioning fingerprint maps. This difficulty arises because smartphone IMUs typically have limited performance, leading to position errors that can reach meter-level inaccuracies within just a few seconds. To tackle this issue, we propose a multi-user joint vehicle dead reckoning post-processing method. The core concept involves constructing virtual observations using vehicle motion information to effectively reduce the position error of the Inertial Navigation System (INS). This includes employing Zero-velocity UPdate Technology (ZUPT) and Non-Holonomic Constraint (NHC). ZUPT constrains the velocity of the INS to zero when the vehicle is stationary, while NHC applies when the vehicle is in motion, ensuring that the lateral and vertical velocities in the vehicle frame are zero. Additionally, the algorithm leverages the consistency of the average magnetic field vector across all vehicle trajectories within the same indoor space to ensure they are roughly aligned in terms of heading. Finally, graph optimization is utilized to integrate these constraints, resulting in a smoother, more accurate, and heading-aligned vehicle trajectory estimation. In this step, the automatic estimation of magnetometer bias is achieved by applying absolute and relative magnetic field constraints. This method addresses the issue of inconsistent magnetometer readings at the same location, which are

caused by different smartphones and their installation positions on the vehicle.

The system state is defined as:

$$X = \{t_{n_i}^k, v_{n_i}^k, R_{nb_i}^k, b_a^k, b_g^k, b_m^k, R_{vb}^k, t_{vb}^k, M_n\} \tag{1}$$

where $t_{n_i}^k$, $v_{n_i}^k$, and $R_{nb_i}^k$ represent the position, velocity, and rotation of the k-th trajectory in the i-th navigation frame (n-frame), respectively, R_{vb}^k and t_{vb}^k represent the rotation and translation from the sensor frame (b-frame) to the vehicle frame (v-frame), b_a^k, b_g^k, and b_m^k represent the accelerometer, gyroscope, and magnetometer bias, respectively, M_n represents the magnetic field vector in the n-frame.

The graph optimization problem of system state estimation is defined as:

$$X = \underset{X}{argmin} \sum e^k + \|r_E(M_n)\|_{\Sigma_E^2} \tag{2}$$

where $r_E(M_n)$ represents the east component of the constraint on the global average magnetic field. This constraint assumes that the east component follows a zero-mean Gaussian distribution, which is essential for ensuring the observability of both the global heading and the global magnetic field vector. It implies that we assume the average magnetic field vector aligns with the local geomagnetic field. e^k defines the cost function used for each trajectory, which is defined as follows:

$$\begin{aligned} e^k = & \sum \|r_{pre}\|_{\Sigma_{pre}}^2 \\ & + \sum \|r_{NHC}\|_{\Sigma_{NHC}}^2 + \sum \|r_{ZUPT}\|_{\Sigma_{ZUPT}}^2 \\ & + \sum \|r_{\overline{M}_n}\|_{\Sigma_{\overline{M}_n}}^2 + \sum \|r_{\Delta\overline{M}_n}\|_{\Sigma_{\Delta\overline{M}_n}}^2 \end{aligned} \tag{3}$$

where r_{pre} represents the relative pose and velocity constraints between consecutive keyframes, which are obtained using IMU pre-integration, with specific forms as detailed in [31].

The NHC approach constructs lateral and vertical zero velocity constraints based on the assumption that a vehicle will not skid or jump during normal driving. However, vehicles often experience varying degrees of vibration due to road irregularities, which can cause the velocity to occasionally violate the NHC assumption. To address this, displacement constraints are derived by integrating the lateral and vertical velocities to mitigate the impact of the vehicle passing over shock-absorbing facilities, whether moving laterally or vertically. In the graph optimization algorithm, the relative posture and velocity obtained through pre-integration are used to generate short-term predictions of relative lateral and vertical displacements in the vehicle's frame of reference, known as the v-frame. The lateral and longitudinal zero displacement constraints in the v-frame is defined as follows:

$$r_{NHC} = A \sum_{j=1}^{k} R_{vb} \left[R_{nb_{i+j}}^T v_{n_{i+j}} + (\omega_{nb_{i+j}}^b \times) t_{vb}^T \right] \Delta T_j - [0,0]^T \tag{4}$$

$$A = \begin{bmatrix} 0 & 1 & 0 \\ 0 & 0 & 1 \end{bmatrix} \tag{5}$$

where R_{vb} and t_{vb} represent the rotation and translation from the sensor frame (b-frame) to the v-frame, $R_{nb_{t+i}}$ and $v_{n_{t+i}}$ represent the rotation and velocity of the i-th epoch after the t-th keyframe, ω_{nb}^b represents the angular rate output by the gyroscope, ΔT_i represents the time interval between two adjacent epochs. The rotation and velocity at time $k+i$ are estimated using pre-integration as follows:

$$R_{nb_{i+j}} = R_{nb_i} R_{b_i b_{i+j}} \tag{6}$$

$$v_{nb_{i+j}} = v_{n_i} + R_{nb_i} v_{b_i b_{i+j}} + g^n \Delta T_{i,i+j} \tag{7}$$

where $R_{b_i b_{i+j}}$, $v_{b_i b_{i+j}}$, and $\Delta T_{i,i+j}$ representing the rotation increment, velocity increment, and the time length from the i-th to the $(i+j)$-th epoch, respectively. It is worth noting that both the mounting angle and the lever arm are variables to be estimated in the residual r_{NHC}. These parameters are highly observable and can be accurately estimated when there is a change in direction of the vehicle motion.

Similarly, when the vehicle is detected to be stationary, the zero displacement constraint is used instead of ZUPT to improve the positioning accuracy. The construction of zero displacement constraints in the n-frame is defined as follows:

$$r_{ZUPT} = \sum_{j=1}^{k} v_{n_{i+j}} \Delta T_j - [0,0,0]^T \tag{8}$$

The magnetic field provides crucial absolute heading information, significantly enhancing trajectory estimation accuracy in multi-user joint VDR post-processing algorithms. However, the vehicle's structure can be a major source of magnetic interference, and indoor environments often present frequent and substantial magnetic disturbances, posing significant challenges to the effective utilization of magnetic fields. In this context, we assume that the smartphone is securely mounted at a specific location within the vehicle. The magnetic interference from the vehicle's structure introduces a relatively stable bias in the magnetometer's readings. We treat this stable bias, combined with the inherent magnetometer bias, as a parameter to be estimated and subsequently eliminated. To address magnetic interference from building structures, we adopt the approach outlined in previous research [31], modeling it as a magnetic field whose errors follow a zero-mean Gaussian white noise distribution. Given that individual user trajectories are typically brief (e.g., around 2 minutes), we integrate the trajectories of all users along with their corresponding magnetic field observations to apply these corrective measures. The constraints for absolute and relative magnetic fields are defined as follows:

$$r_{\overline{M}_n} = R_{nb_i} \overline{M}_{b_i} - M_n \tag{9}$$

$$r_{\Delta\overline{M}_n} = R_{nb_i} \overline{M}_{b_i} - R_{nb_j} \overline{M}_{b_j} \tag{10}$$

$$\overline{M}_{b_i} = \frac{1}{N} \sum_{s}^{N} R_{b_i b_{i+s}} (M_{b_{i+s}} - b_m) \tag{11}$$

where $r_{\overline{M}_n}$ represents the absolute magnetic field constraint, which is related to the attitude and magnetometer bias of all trajectories and the global magnetic field. Since the vehicle trajectories typically cover large areas, this constraint enforces approximate heading alignment among all trajectories. This property arises because large-area magnetic field measurements naturally suppress heading drift, even in areas with significant magnetic field disturbances, as demonstrated in prior work [31]. $r_{\Delta\overline{M}_n}$ represents the relative magnetic field

constraint, which is related to the attitude and magnetometer bias of a single trajectory. Since the sensor rotates about two different axes, effectively simulating the magnetometer bias error in the trajectory, this constraint can effectively achieve accurate estimation of the magnetometer bias by exploiting the short-term consistency of the magnetic field.

To prevent convergence to local minima, we employ a Kalman filter-based vehicle dead reckoning method to estimate the vehicle's initial trajectory. Building on this foundation, solving (2) yields a smooth three-dimensional vehicle trajectory. The optimization algorithm leverages the global average magnetic field constraint measured along each trajectory to roughly align the headings of all trajectories. Additionally, the cost function incorporates both absolute and relative magnetic field constraints to ensure the precise estimation of magnetometer bias. This accuracy is crucial for utilizing the magnetic field sequence associated with all trajectories for keyframe association.

IV. Global Trajectory Optimization

Due to the performance limitations of the built-in IMU in smartphones, the 3D vehicle trajectory produced by VDR is prone to significant positional errors. To address this, we employ a global trajectory optimization approach that integrates both inequality and equality constraints in a tightly-coupled manner, akin to the crowdsourced pedestrian trajectory estimation method described in [29]. In the inequality constraint optimization phase, we estimate only the initial 3D position and heading of each trajectory. We leverage the heading information derived from the global average magnetic field vector to provide an initial pose and a keyframe association correctness marker, which remain unaffected by any keyframe association errors. During the equality constraint optimization phase, we utilize the original IMU observations to impose constraints, thereby preventing the loss of information that might occur if we were to rely solely on the relative poses between keyframes as output by VDR.

A. Inequality Constraint Optimization

Even with constraints based on the average magnetic field, the headings of crowdsourced trajectories estimated using VDR still exhibit varying degrees of inconsistency. Moreover, due to the limited number of trajectories and the strong correlation between magnetic field perturbations and specific spatial regions, modeling the heading error as Gaussian noise proves to be less effective. To address this, we employ inequality constraints derived from magnetic field heading information to account for variations in magnetic heading caused by differing magnetic field perturbations across the regions traversed by each trajectory.

The three-dimensional trajectory optimization problem, incorporating inequality constraints, is defined as follows:

$$\{t^k, \psi^k\} = \underset{t^k,\psi^k}{argmin} \sum \rho_{Cauchy}(\|r_{Dis}\|_{\Sigma^2_{Dis}}) \quad s.t. \psi^k_{low} < \psi^k < \psi^k_{upper} \tag{12}$$

where p_k and ψ^k represent the trajectory three-dimensional position and heading in the n-frame, ψ^k_{low} and ψ^k_{upper} are the boundaries of heading fluctuations, which are empirically set to $\pm 20°$.

$$\rho_{\text{Cauchy}}(s) = log\,(1 + s) \tag{13}$$

The Cauchy kernel function exhibits a smaller gradient for larger residuals compared to the Huber kernel function. This characteristic implies that the optimization process utilizing the Cauchy kernel function is less prone to errors arising from incorrect keyframe associations. To reduce the dimensionality of the system state that needs to be estimated, and consequently decrease the computational burden, we represent all keyframes of the trajectory using the pose of the initial keyframe along with the relative poses provided by the VDR. The cost function, denoted as r_{Dis}, imposes a constraint on the three-dimensional distance between two keyframes:

$$r_{\text{Dis}} = \left(R\left(\psi^k_0\right) t^{k,p}_n + t^k_{n_0}\right) - \left(R(\psi^l_0) t^{l,q}_n + t^l_{n_0}\right) \tag{14}$$

$$R\left(\psi_0\right) = \begin{bmatrix} cos\psi_0 & -sin\psi_0 & 0 \\ sin\psi_0 & cos\psi_0 & 0 \\ 0 & 0 & 1 \end{bmatrix} \tag{15}$$

where $t^k_{n_0}$ and ψ^k_0 represent the translation and rotation angle of the k-th trajectory, respectively, $t^{k,p}_n$ represents the position of the p-th keyframe of the k-th trajectory.

The problem is addressed iteratively using the Levenberg-Marquardt (LM) algorithm, as detailed in the foundational works by Levenberg [32] and Marquardt [33]. Once (12) is solved, the algorithm updates the pose and velocity of each keyframe in the trajectory with the following equations:

$$R^k_{nb_i} = R(\psi^k) R^k_{nb_i} \tag{16}$$

$$t^k_{n_i} = R(\psi^k) t^k_{n_i} + t^k_{n_0} \tag{17}$$

$$v^k_{n_i} = R(\psi^k) v^k_{n_i} \tag{18}$$

B. Equality Constraint Optimization

Inequality constraint optimization is used to determine the initial pose of each trajectory and to verify the accuracy of keyframe associations. Building on this foundation, a tightly coupled optimization process refines the trajectory estimates by leveraging constraints from the IMU within a trajectory, loop closure detection across multiple trajectories, and clustering of elevation constraints for the same floor. Given the low accuracy of VDR in estimating elevation, this method employs the consistent height of vehicles on the same floor to formulate elevation constraints. The global optimization problem is defined as follows:

$$X = \underset{X}{argmin}\{e^k + \| r_{tLC} \|^2_{\Sigma_{tLC}} + \| r_{mLC} \|^2_{\Sigma_{mLC}} + \| r_{floor} \|^2_{\Sigma_{floor}} + \| r_E(M_n) \|^2_{\Sigma_E}\} \tag{19}$$

where e^k represents the constraints within each trajectory, as defined in Eq. (3), $r_E(M_n)$ represents the east component constraint of the global average magnetic field, which ensures the observability of the global heading and magnetic field vector.

r_{tLC} represents the position revisit constraint (i.e. loop closure) between keyframes, which is defined as:

$$r_{tLC} = (R_{nb}^{k,p} t_b^k + t_n^{k,p}) - (R_{nb}^{l,q} t_b^l + t_n^{l,q}) \tag{20}$$

where $t_{n\kappa_i}^k$ and $R_{nb_i}^k$ represent the position and rotation of the i-th keyframe of the k-th trajectory, t_b^k is the alignment point in the b-frame of the i-th keyframe. The alignment points between two keyframes are determined by calculating the correlation of magnetic field sequences. Given that keyframes are extracted at equal intervals of 1 second, the spatial resolution of keyframes in underground parking scenarios ranges from approximately 2 to 8 meters. This variability makes it challenging to ensure a strict overlap between alignment points and keyframes. The conversion relationship between an alignment point and a keyframe can be expressed as follows:

$$t_b^k = (R_{n_0 b}^{k,p})^T \left(t_{n_i}^k - t_{n_0}^{k,p}\right) \tag{21}$$

where $t_{n_0}^{k,p}$ and $R_{n_0 b}^{k,p}$ represent the position and rotation of the p-th keyframe of the k-th trajectory, respectively, and $t_{n_i}^k$ represents the position of the alignment point, corresponding to the i-th sample of the k-th trajectory. These parameters are estimated through multi-user joint VDR. It is important to note that in pedestrian scenarios, the correction of the aforementioned closed-loop position constraint is not necessary. This is because pedestrians typically move about 1 meter per second, and choosing the nearest keyframe results in a closed-loop position deviation of only around 1 meter. Additionally, the accuracy of pedestrian dead reckoning is relatively low. Due to these factors, the crowdsourced trajectory estimation for pedestrians, as discussed in [29], is not significantly affected by the potential misalignment between alignment points and keyframes.

r_{mLC} represents the magnetic field vector constraint at the alignment point, defined as:

$$r_{mLC} = R_{nb}^{k,p} R_{bb_i}^k (M_{b_i}^k - b_m^k) - R_{nb}^{l,q} R_{bb_j}^l (M_{b_j}^l - b_m^l) \tag{22}$$

where $R_{bb_i}^k$ and $R_{bb_j}^l$ represent the relative rotation from the alignment point to the keyframe, which come from the multi-user joint VDR, b_m^k and b_m^l represent the magnetometer biases for the two trajectories, $M_{b_i}^k$ and $M_{b_j}^l$ represent the magnetometer measurements at the alignment point, which are obtained by linear interpolation of the original magnetometer measurements.

The consistency constraint of the magnetic field vector at the alignment point is inherently present when a loop closure is established, and its reliability surpasses that of the aforementioned absolute and relative magnetic field constraints. While the absolute constraint reduces noise impact on individual cost functions through global averaging, and the relative constraint is less influenced by spatial distribution differences of magnetic field disturbances, both are still affected by spatial position-related magnetic field disturbances. This results in a constraint covariance that is necessarily greater than the magnetometer measurement noise. In the context of r_{mLC}, the alignment of the magnetic field sequence ensures that the difference between measurements at two moments is almost independent of magnetic field disturbances. Consequently, its covariance can be considered to be solely within the bounds of magnetometer measurement noise, making the constraint more stringent. This constraint guarantees that magnetic field vectors at the same spatial location remain consistent across different trajectories, thereby further ensuring the consistency of magnetometer bias estimation within the data of each trajectory.

r_{floor} represents the floor constraint, assuming that the error in estimating trajectory height on the same floor follows a zero-mean Gaussian distribution.

$$r_{floor} = [t_n^{k,p}]_z - \bar{z}_{floor} \tag{23}$$

where $[t_n^{k,p}]_z$ represents the elevation of the p-th keyframe of the k-th trajectory; $\bar{z}_{floor}$ represents the average floor elevation. The establishment of the floor elevation constraint relies on floor clustering, which effectively mitigates inconsistencies in elevations across different trajectories. Notably, even keyframes that are not initially assigned to the correct floor can have their elevations indirectly adjusted through the floor elevation constraints applied to other keyframes within the same trajectory. Global graph optimization and floor clustering typically involve multiple iterations during the optimization process. As a result, the elevations of keyframes not correctly assigned in the current optimization round may already be nearing the accurate floor height. In subsequent optimization rounds, these keyframes might be correctly identified by floor clustering as belonging to the appropriate floor. Ultimately, the elevations of keyframes exhibiting horizontal movement will gradually converge to the correct floor height.

The floor clustering algorithm is employed to ascertain and reconstruct floor heights using crowdsourced vehicle trajectories, addressing the limitations in vertical position accuracy inherent in VDR. Prior to initiating floor clustering, keyframes are categorized as either planar or non-planar, with only those marked as planar being utilized in the analysis. Given the limited reliability of VDR's vertical velocity and displacement data, we rely on the vehicle's pitch to determine whether it is traveling on a specific floor. The criteria for this assessment are as follows:

$$\frac{1}{n}\sum_{i=1}^{n} \theta_i < \gamma_\theta \tag{24}$$

$$\theta = tan^{-1} \frac{[R_{nv}]_{3,1}}{\sqrt{\left([R_{nv}]_{3,2}\right)^2 + \left([R_{nv}]_{3,3}\right)^2}} \tag{25}$$

where $R_{nv} = R_{nb} R_{vb}^T$ represents the rotation from the v-frame to the n-frame, $[\cdot]_{3,1}$ represents represents the 3-th row and 1-th column of the matrix, γ_θ represents the threshold set based on experience.

Based on Equation 24, keyframes that move on a plane are selected, and the floor clustering method groups these keyframes by floor to minimize the height estimation error in the trajectory. Figure 2 illustrates the detailed process of floor clustering, which includes generating a height distribution histogram, selecting cluster centers, and labeling samples for each cluster. The specific steps are as follows:

Step 1: The height of each keyframe is extracted using the vertical position data from the VDR trajectory output.

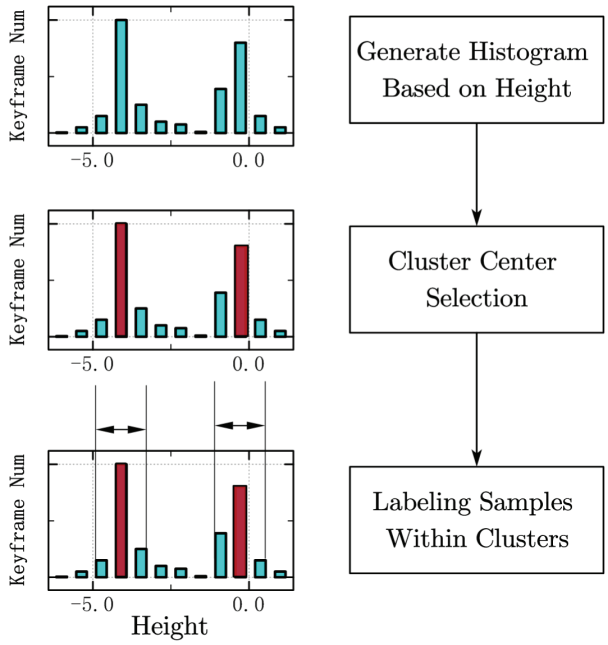

Fig. 2. The flowchart of the floor clustering method. The left side shows the height histogram processing flow.

A height distribution histogram is then constructed for all keyframes, utilizing a bin size of 0.5 meters.

Step 2: A peak detection algorithm, enhanced with non-maximum suppression, is employed to accurately identify the peaks in the histogram.

Step 3: The average height of all samples within each identified peak is calculated to represent the average floor height, denoted as $\bar{z}_{floor}$.

The proposed method uses loop constraints to transfer elevation information between trajectories, ensuring that the elevation estimates of all trajectory data are uniform and accurate. Through the iterative cycle of underlying clustering and global trajectory optimization, each time a trajectory segment is accurately clustered, its elevation parameters are appropriately constrained. In addition, the elevation values of other trajectories linked by loop constraints are also adjusted synchronously. In the subsequent clustering stage, these trajectories with improved elevation accuracy will obtain higher-precision clustering results, thus establishing a self-reinforcing improvement mechanism in the entire optimization process.

V. Experiments and Results

A. Experiment Description

The verification and evaluation experiments for this study were conducted in two three-story underground parking lots: one at a shopping mall and the other at a school dormitory building. Due to space constraints on the first underground floor, the experiments were limited to the second and third floors. A point cloud representation of the experimental setting is provided in Fig. 3. In Scenario 1, the second underground floor of the parking lot covers approximately 14,000 square meters, while the third floor spans about 7,000 square meters.

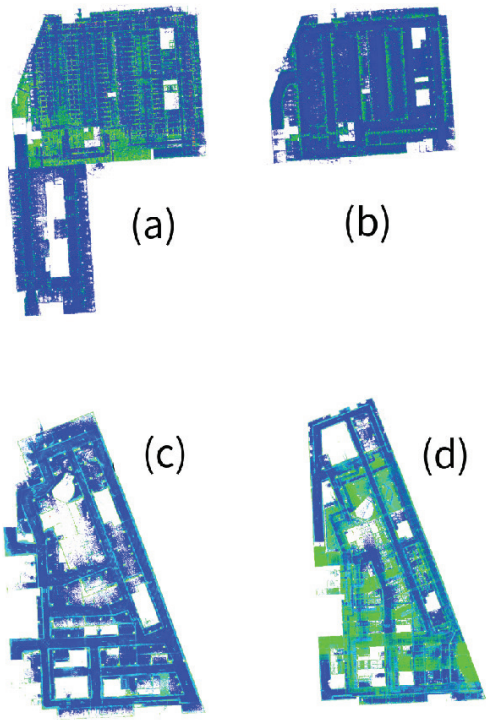

Fig. 3. Point Cloud of Experiment Scenario 1 and Scenario 2. (a) and (b) are the second and third underground floor in scene 1, (c) and (d) are the second and third underground floor in scene 2.

In Scenario 2, both the second and third underground floors of the parking lot each cover approximately 20,000 square meters.

Given the legal restrictions associated with crowdsourced data collection in real-world scenarios, such as concerns over personal privacy, we simulated crowdsourced vehicle data by actively collecting data from smartphones within vehicles. For detailed data collection guidelines, please refer to Sec V-B. The dataset includes specific data such as the true trajectory obtained from a laser SLAM system mounted on the vehicle. This system ensures that the reference trajectory maintains a consistency better than 5 cm, which is sufficient for evaluating the crowdsourced mapping algorithm discussed in this study.

B. Crowdsourced Dataset Simulation

The characteristics and parameters of the simulated dataset are outlined as follows:

- **Sensor Configuration**: The dataset comprises GNSS positions recorded at a data rate of 1 Hz, along with uncalibrated gyroscope, accelerometer, and magnetometer observations recorded at 100 Hz. Given that only about 30% of smartphones are equipped with a barometer, the proposed method excludes barometer observations. To account for variations in smartphone hardware, data collection was conducted using three different smartphones: two Huawei Mate 40 Pro devices and one Xiaomi 11. The dataset spans approximately 4 hours for Scenario 1 and 5 hours for Scenario 2.
- **Smartphone Installation**: In line with common practices for using smartphones in vehicle navigation, the

Fig. 4. The installation position of the smartphone in the vehicle. Only the sensor data of one smartphone is used in a single test.

smartphones in the dataset were mounted on brackets attached to the vehicle windshield, as illustrated in Fig. 4. Since the bracket allows for a high degree of freedom, the installation posture of the smartphone was not restricted to align with the vehicle's moving direction, reflecting typical user habits. To address potential performance degradation in vehicle dead reckoning due to changes in the smartphone's position and orientation, the proposed method integrates GNSS data, vehicle motion constraints, and sensor observations to achieve automatic estimation and compensation.

- **Vehicle Dynamic**: A user drives a vehicle from an outdoor area into the indoor parking lot, makes a brief stop, and then exits. This process is divided into two stages. In the first stage, the vehicle reaches the parking lot entrance, stops for a few seconds for authentication, drives to a parking space, and stops again briefly. In the second stage, the vehicle is started, pauses for a safety check, drives to the exit, and stops for authentication. Each continuous trajectory between the parking space and the entrance/exit is treated as an independent sample, with the trajectories from the first and second stages considered as two separate samples. To account for variations in driving habits, three drivers participated in data collection, with no restrictions on their specific driving behaviors. Additionally, to enhance dataset coverage within the parking lots, parking spaces were selected to ensure even distribution, maximizing route diversity and full coverage of the parking area.

C. Evaluation Metric

The test data with reference truth is divided into two parts for evaluation purposes: the first part of the test data is dedicated to assessing the accuracy of the crowdsourced magnetic field map. This segment consists of approximately 20 minutes of data in Scenario 1 and 45 minutes in Scenario 2, and the second part of the test data is used to evaluate the accuracy of magnetic positioning utilizing the constructed magnetic map. This segment includes about 7 minutes of data in Scenario 1 and 10 minutes in Scenario 2.

The estimated positions for the trajectories in the first part are represented as $\{\hat{t}_0, \ldots, \hat{t}_N\}$, while the corresponding reference positions are denoted as $\{t_0, \ldots, t_N\}$. The position error E_m of the estimated trajectory and the positioning error

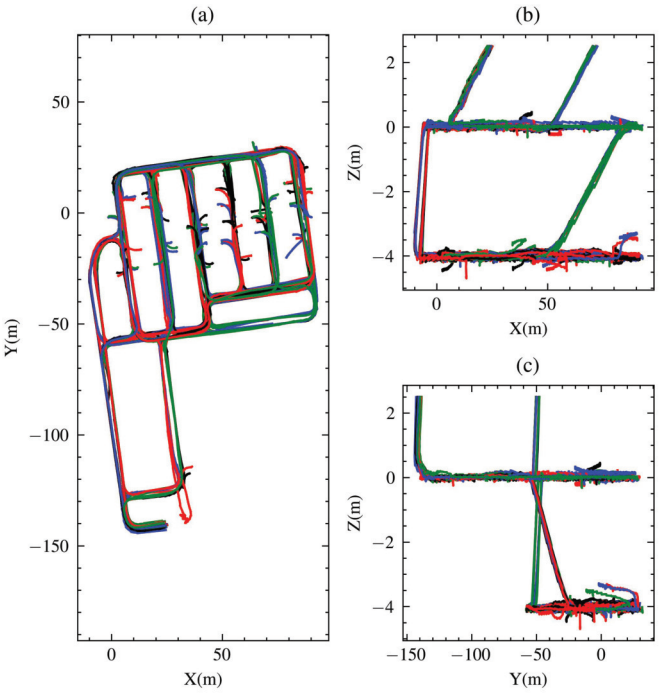

Fig. 5. All vehicle trajectories in the dataset estimated by the proposed method in scenario 1. Lines of different colors represent the different vehicle trajectories.

E_p based on the magnetic sequence matching are used to evaluate the performance of the proposed method.

The position error E_m is defined as:

$$E_m = \frac{1}{N} \sum_{i \in [0,N]} \|R_a(\hat{t}_i - t_a) - t_i\| \tag{26}$$

where

$$\{R_a, t_a\} = \arg\min_{\{R_a, t_a\}} \sum_{i \in [0,N]} \|R_a(\hat{t}_i - t_a) - t_i\| \tag{27}$$

$\|\cdot\|$ is $l2$-norm. R_a and t_a are 2D rotation and translation, respectively.

E_p is the positioning error using the built magnetic sequence fingerprint map that is alignment with the reference framework using (26). The positioning method is a brute force sequence-matching-based method [34], and a magnetic field sequence withing the distance of 25 meters of the keyframe. E_p is defined as:

$$E_p = \frac{1}{N} \sum_{i \in [0,N]} \|\hat{t}_i^{\prime} - t_i\| \tag{28}$$

where $\hat{t}_i^{\prime}$ is positioning results, t_i is reference position.

D. Performance Evaluation

Figure 5 illustrates all vehicle trajectories in the dataset as estimated by the proposed method in Scenario 1. Subfigures (a), (b), and (c) represent the top, front, and side views, respectively. Different colors are used to denote distinct vehicle trajectories; however, due to the large number of trajectories, colors are reused. In Figure 5(a), the estimated

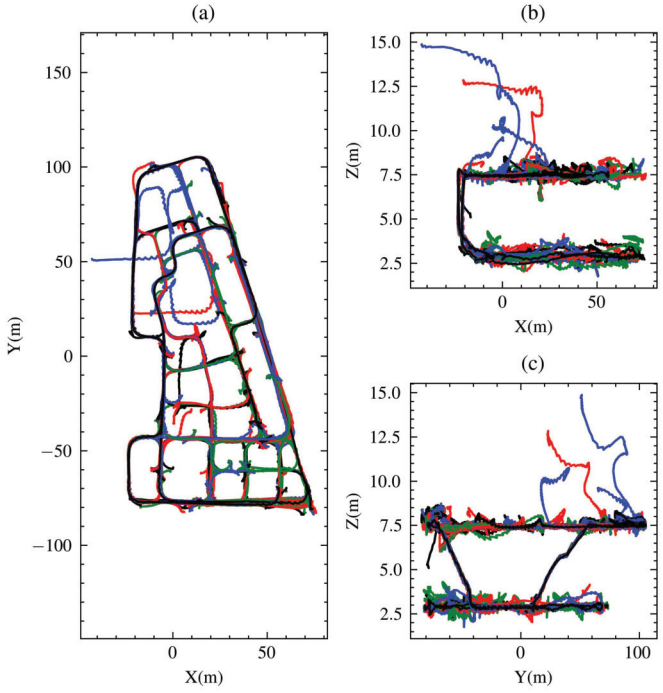

Fig. 6. All vehicle trajectories in the dataset estimated by the proposed method in scenario 2. Lines of different colors represent the different vehicle trajectories.

vehicle trajectories appear very smooth, and the overlap of different trajectories within the same lane is so precise that it becomes difficult to distinguish the floor level from a bird's-eye view. In Figures 5(b) and (c), the floors on which the trajectories are located and the transitions between them are clearly visible. The height fluctuations of most vehicle trajectories within a single floor are minimal, typically only a few decimeters. Figure 6 displays all vehicle trajectories in the dataset as estimated by the proposed method in Scenario 2. The trajectories in Scenario 2 are generally similar to those in Scenario 1. However, several noticeable abnormal trajectories are present in Scenario 2. These anomalies are primarily due to the poor quality of the smartphone's built-in sensor and its mounting under the front windshield using a bracket. Although the proposed algorithm includes a floor clustering method, it does not strictly fix the height of vehicle trajectories on a single floor due to slight slopes in real-world scenarios. As a result, the algorithm may encounter potential inaccuracies under these combined interference factors. Fortunately, during the generation of magnetic maps, a screening mechanism is employed to eliminate such abnormal trajectories, thereby mitigating their impact on magnetic matching positioning.

Figure 7 illustrates the test vehicle trajectories estimated by the proposed method. These estimated trajectories align well with the reference trajectories, demonstrating a high degree of overlap in their planar shapes. Notably, there is no significant scale error in the estimated vehicle trajectories, which marks an improvement over our previous work involving magnetic map construction based on crowdsourced pedestrian data [29]. This improvement can be attributed to the relatively stable dynamics of the smartphone when used in a vehicle, compared

TABLE I

THE MEAN, 68%, AND 95% OF THE POSITION ERRORS OF THE TEST TRAJECTORIES AND MAGNETIC MATCHING POSITIONING (UNIT: M)

Test	Trajectory Position			Trajectory Height			Matching Position		
	Mean	68%	95%	Mean	68%	95%	Mean	68%	95%
1	1.40	1.51	2.75	0.18	0.26	0.41	1.17	1.32	2.29
2	0.96	1.11	1.80	0.23	0.28	0.59	1.16	1.41	2.13

to the more variable manner in which pedestrians hold their devices. The simpler dynamics allow the VDR to effectively utilize vehicle motion constraints, resulting in more reliable relative position estimation. Additionally, VDR offers dependable altitude estimation, with an error margin of only a few decimeters—an accuracy level that is challenging to achieve with Pedestrian Dead Reckoning (PDR).

Figure 8 presents the magnetic matching positioning results based on the crowdsourced magnetic sequence fingerprint map. Visually, these positioning results show good consistency with the reference data, although they do not completely overlap. There are systematic fixed deviations, particularly in the elevation direction. These deviations are primarily due to factors such as the low quality of smartphone sensors and variations in vehicle motion, which introduce unavoidable disturbances in the magnetic sequence fingerprint map generated from crowdsourced vehicle trajectories. Additionally, flat areas persist in the magnetic features of the underground parking lot, influenced by the presence of ferromagnetic objects in the environment. The limited width of the lanes in the underground parking lot further contributes to this issue, as the magnetic field features along the sides of the lanes provide weak positional perception.

Figures 9 and 10 display the Cumulative Density Function (CDF) of position errors for the test trajectories and magnetic matching positioning. Table I provides the mean, 68%, and 95% position errors for both the test trajectories and magnetic matching positioning. In scenario 1, the horizontal and height errors of the estimated vehicle trajectory are 2.75 meters (95%) and 0.41 meters (95%), respectively. The matching positioning error of the crowdsourced magnetic sequence map is 2.29 meters (95%). In scenario 2, the horizontal and height errors of the estimated vehicle trajectory are 1.18 meters (95%) and 0.59 meters (95%), respectively. The matching positioning error of the crowdsourced magnetic sequence fingerprint map is 2.13 meters (95%). The estimation accuracy of vehicle trajectories in both scenarios is comparable, with an elevation accuracy better than 0.6 meters. This indicates that the proposed method is highly adaptable and capable of accurately estimating crowdsourced vehicle 3D trajectories. The magnetic matching positioning accuracy is comparable to, or even slightly better than, the estimation accuracy of the crowdsourced vehicle trajectories. This is because the vehicle trajectories used in the evaluation represent only a small portion of the dataset, whereas the magnetic matching positioning stage utilizes the complete dataset and data filtered by preset criteria to generate the magnetic sequence fingerprint map.

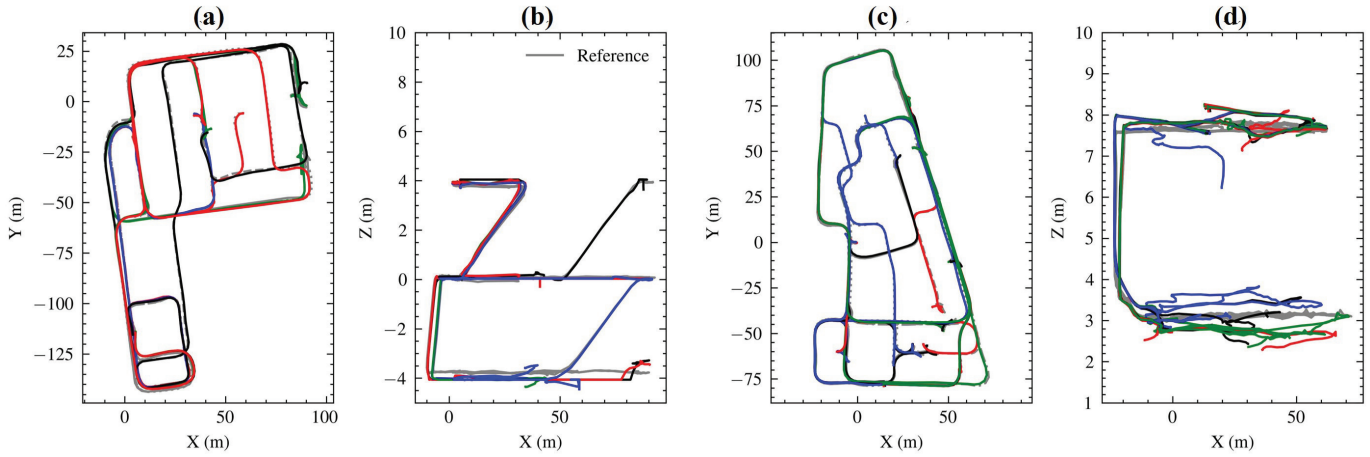

Fig. 7. The test vehicle trajectories estimated by the proposed method. The reference trajectories are represented in gray, and the estimated trajectories are represented in other colors. (a) and (b) are for scenario 1, (c) and (d) are for scenario 2.

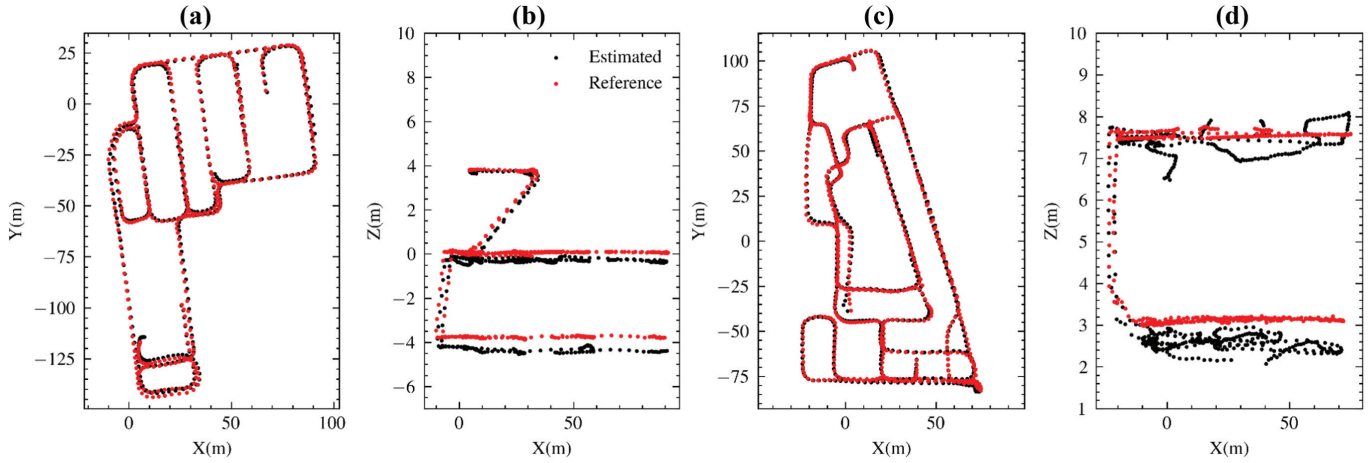

Fig. 8. Magnetic matching positioning results based on the crowdsourced magnetic sequence map. The red points are references, and the black points are magnetic matching positioning results. (a) and (b) are for scenario 1, (c) and (d) are for scenario 2.

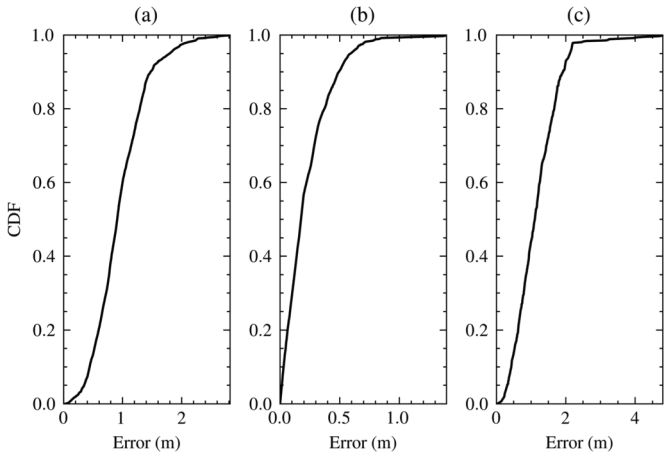

Fig. 9. The Cumulative Density Function of position errors of the test trajectories and magnetic matching positioning for scenario 1.

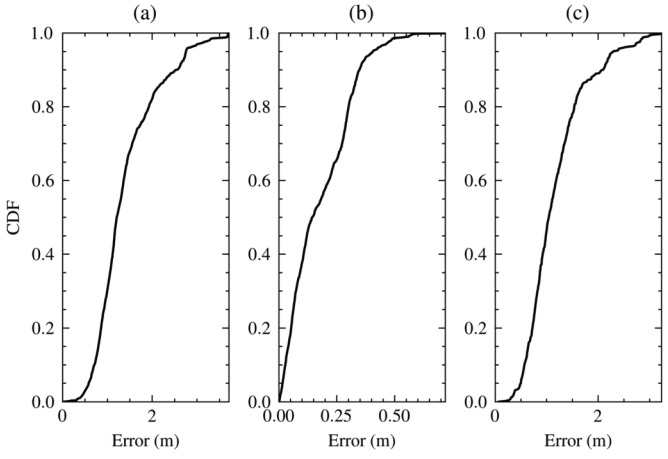

Fig. 10. The Cumulative Density Function of position errors of the test trajectories and magnetic matching positioning for scenario 2.

Based on the test results, it is evident that the proposed method can accurately determine 3D vehicle trajectories using only crowdsourced smartphone sensor data from vehicles. This method effectively supports vehicle users in obtaining

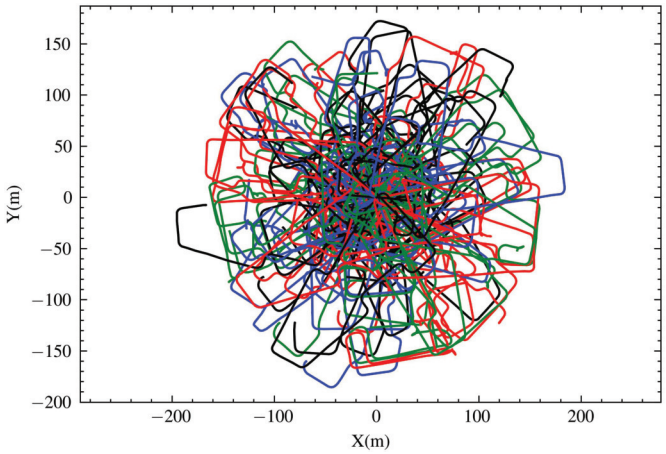

Fig. 11. All vehicle trajectories in the dataset estimated by the traditional VDR in scenario 2. Lines of different colors represent the different vehicle trajectories.

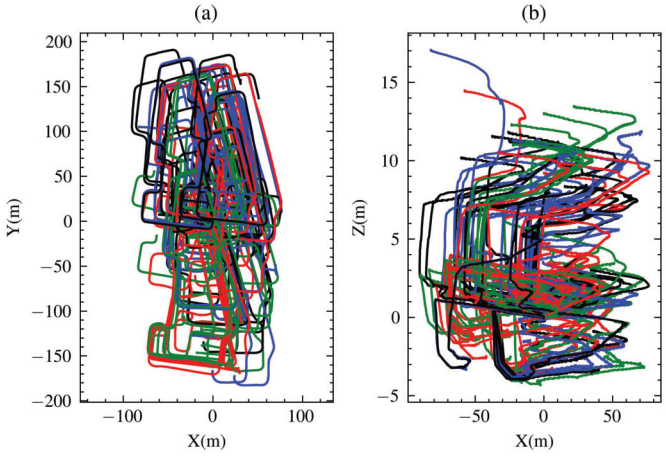

Fig. 12. All vehicle trajectories in the dataset estimated by the proposed multi-user joint VDR in scenario 2. Lines of different colors represent the different vehicle trajectories. (a) Top view, (b) Side view.

meter-level accuracy for indoor magnetic field matching positioning services.

E. Ablation Experiment

Figures 11 and 12 illustrate all vehicle trajectories in the dataset, estimated by the traditional VDR and the proposed multi-user joint VDR in scenario 2, respectively. All trajectories are initialized at the origin with a starting heading of zero. The multi-user joint VDR algorithm incorporates a global magnetic field vector constraint on the vehicle heading, resulting in trajectories that demonstrate clear consistency in heading direction. Despite the magnetic interference from the vehicle's metal structure and electronic equipment, the global magnetic field vector constraint remains effective after correcting for the equivalent magnetometer bias. This ensures improved heading accuracy and trajectory consistency across multiple users.

Compared to the multi-user joint PDR for constructing magnetic field maps using crowdsourced pedestrian data (as discussed in our previous work [29]), the multi-user joint

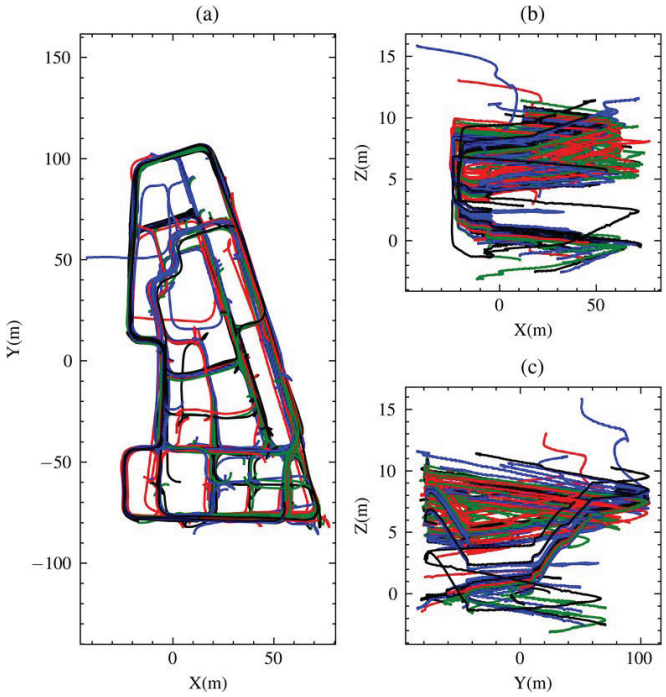

Fig. 13. All vehicle trajectories in the dataset estimated by the inequality constraint optimization in scenario 2. Lines of different colors represent the different vehicle trajectories. (a) Top view, (b) and (c) Side view.

VDR offers significant accuracy advantages. The reasons for this improved accuracy include: 1) Vehicles move faster than pedestrians, allowing them to cover the same distance in a shorter time. This results in higher relative accuracy for pure gyroscope integration due to the reduced accumulation of errors over time. 2) A single vehicle's trajectory is typically longer and covers a larger area. This extensive coverage means the global magnetic field vector is less susceptible to localized magnetic field interference, enhancing the reliability of the data. 3) VDR provides more accurate estimates of the horizontal attitude angle, which is crucial for using the magnetic field vector effectively in accurate heading estimation. 4) Smartphones installed in vehicles often benefit from more stable and consistent mounting conditions. Additionally, the vehicle's predictable motion pattern can be leveraged to better constrain the heading, further improving accuracy.

Despite the advantages of the multi-user joint VDR, it does not fully restore the relative relationships between different trajectories and struggles with low height estimation accuracy for vehicle trajectories. NHC constrains the vertical and lateral velocities in the vehicle frame to zero. In the underground garage dataset analyzed in this paper, the vehicle undergoes frequent heading changes, leading to continuous corrections of horizontal velocity in the navigation frame. However, the projection of the vehicle's vertical direction in the navigation frame shows minimal variation and lacks periodic error compensation characteristics, resulting in a continuous accumulation of elevation error over time. Furthermore, frequent speed bumps and other indoor obstacles cause vertical vehicle oscillations, undermining the NHC assumption and negatively impacting vertical positioning accuracy.

Collectively, these factors compromise the stability of NHC and ultimately degrade vertical positioning performance. Figure 13 illustrates all vehicle trajectories in the dataset, estimated using inequality constraint optimization in scenario 2. The magnetic feature-based trajectory keyframe association provides accurate relative constraints between trajectories. Building on this, the inequality global optimization effectively restores the planar coordinates of vehicle trajectories, allowing for clear lane differentiation. However, the height estimation for vehicle trajectories, as depicted in Figures 13 (b) and (c), remains inaccurate. This inaccuracy is primarily due to the irregular distribution of speed bumps and manhole covers in the underground parking lot, which cause significant smartphone vibrations. As a result, the benefits of vehicle motion constraints in the elevation direction are greatly diminished. To address this issue, an elevation clustering algorithm has been integrated into the global trajectory optimization process. By defining the optimization problem through multiple iterations, as shown in Figure 6, the accuracy of vehicle trajectory estimation is further enhanced. This iterative approach helps mitigate the effects of vertical disturbances and improves the reliability of height estimations.

In summary, the multi-user joint VDR effectively captures crowdsourced vehicle trajectories with consistent headings, which significantly supports the feasibility of the proposed method. Building on this foundation, trajectory optimization with inequality constraints enhances the reliability of trajectory correlation information, which would otherwise depend solely on magnetic features. Furthermore, by employing global trajectory optimization with equality constraints, the method achieves precise estimation of crowdsourced vehicle trajectories and facilitates the generation of accurate magnetic sequence maps. This comprehensive approach ensures improved accuracy and reliability in mapping vehicle movements and the surrounding magnetic field.

VI. Conclusion and Future Work

Indoor magnetic matching is a viable method for navigating multi-floor parking lots, but it requires reducing mapping costs through the use of crowdsourced data. To tackle this challenge, this paper introduces a novel approach for constructing a magnetic map using crowdsourced vehicle data. Initially, the method employs a multi-user joint Vehicle Dead Reckoning (VDR) based on graph optimization, which establishes incremental vehicle motion constraints and magnetic field vector consistency constraints within the same space. This process results in the estimation of crowdsourced vehicle trajectories with consistent directions. Subsequently, the method constructs associations between different vehicle trajectories using the multi-attribute characteristics of the magnetic field. Finally, a two-step global trajectory optimization method incorporating inequality and equality constraints is proposed. The inequality constraint streamlines the optimization process, allowing for quick verification of trajectory correlation information and the acquisition of accurate initial values. Building on this, the equality constraint iteratively refines the optimization problem to achieve precise estimation of crowdsourced vehicle trajectories and the generation of magnetic sequence fingerprint maps.

The test results from simulated data in two three-story underground parking lots demonstrate that the proposed method, utilizing only on-board smartphone sensor data, achieves plane and elevation errors in the crowdsourced vehicle trajectory estimation of less than 2.75 meters (95%) and 0.59 meters (95%), respectively. Furthermore, the magnetic matching positioning error, based on crowdsourced magnetic sequence maps, is less than 2.29 meters (95%). These findings confirm the feasibility of the proposed method and indicate that the magnetic sequence fingerprint map generated from crowdsourced vehicle data can effectively support meter-level indoor positioning services.

The test results in this paper utilize user-active data to simulate crowdsourced vehicle data, maintaining an ideal state for smartphone data. However, in real-world scenarios, crowdsourced in-vehicle smartphone data is often complex, with significant amounts of abnormal and unavailable data, presenting a challenge for the proposed method. In the future, we plan to use in-vehicle smartphone data from actual users driving in real-world conditions to assess the performance of the proposed method. This will allow us to further iterate and optimize the method to better handle the complexities and variability of real-world data.

References

[1] N. El-Sheimy and Y. Li, "Indoor navigation: State of the art and future trends," *Satell. Navigat.*, vol. 2, no. 1, pp. 1–23, Dec. 2021.

[2] J. Einsiedler, I. Radusch, and K. Wolter, "Vehicle indoor positioning: A survey," in *Proc. 14th Workshop Positioning, Navigat. Commun. (WPNC)*, Oct. 2017, pp. 1–6.

[3] Z. Xiao, Y. Chen, M. Alazab, and H. Chen, "Trajectory data acquisition via private car positioning based on tightly-coupled GPS/OBD integration in urban environments," *IEEE Trans. Intell. Transp. Syst.*, vol. 23, no. 7, pp. 9680–9691, Jul. 2022.

[4] V. Havyarimana, Z. Xiao, T. Semong, J. Bai, H. Chen, and L. Jiao, "Achieving reliable intervehicle positioning based on redheffer weighted least squares model under multi-GNSS outages," *IEEE Trans. Cybern.*, vol. 53, no. 2, pp. 1039–1050, Feb. 2023.

[5] T. Qin, Y. Zheng, T. Chen, Y. Chen, and Q. Su, "A light-weight semantic map for visual localization towards autonomous driving," in *Proc. IEEE Int. Conf. Robot. Autom. (ICRA)*, May 2021, pp. 11248–11254.

[6] Z. Bao, S. Hossain, H. Lang, and X. Lin, "A review of high-definition map creation methods for autonomous driving," *Eng. Appl. Artif. Intell.*, vol. 122, Jun. 2023, Art. no. 106125.

[7] A. T. Abraha and B. Wang, "MRILoc: Multiresolution indoor localization from crowdsourced samples," *Pervas. Mobile Comput.*, vol. 87, Dec. 2022, Art. no. 101719. [Online]. Available: https://www.sciencedirect.com/science/article/pii/S1574119222001328

[8] Z. Li, X. Zhao, Z. Zhao, and T. Braun, "WiFi-RITA positioning: Enhanced crowdsourcing positioning based on massive noisy user traces," *IEEE Trans. Wireless Commun.*, vol. 20, no. 6, pp. 3785–3799, Jun. 2021.

[9] M. Ibrahim et al., "Wi-go: Accurate and scalable vehicle positioning using WiFi fine timing measurement," in *Proc. 18th Int. Conf. Mobile Syst., Appl., Services*, Jun. 2020, pp. 312–324.

[10] A. Mackey, P. Spachos, L. Song, and K. N. Plataniotis, "Improving BLE beacon proximity estimation accuracy through Bayesian filtering," *IEEE Internet Things J.*, vol. 7, no. 4, pp. 3160–3169, Apr. 2020.

[11] J. Kuang, T. Li, Q. Chen, B. Zhou, and X. Niu, "Consumer-grade inertial measurement units enhanced indoor magnetic field matching positioning scheme," *IEEE Trans. Instrum. Meas.*, vol. 72, pp. 1–14, 2023.

[12] J. Kuang, X. Niu, P. Zhang, and X. Chen, "Indoor positioning based on pedestrian dead reckoning and magnetic field matching for smartphones," *Sensors*, vol. 18, no. 12, p. 4142, Nov. 2018.
[13] W. Wang, D. Marelli, and M. Fu, "Multiple-vehicle localization using maximum likelihood Kalman filtering and ultra-wideband signals," *IEEE Sensors J.*, vol. 21, no. 4, pp. 4949–4956, Feb. 2021.
[14] C. Zhao, A. Song, Y. Zhu, S. Jiang, F. Liao, and Y. Du, "Data-driven indoor positioning correction for infrastructure-enabled autonomous driving systems: A lifelong framework," *IEEE Trans. Intell. Transp. Syst.*, vol. 24, no. 4, pp. 3908–3921, Apr. 2023.
[15] V. Girbés-Juan, L. Armesto, D. Hernández-Ferrándiz, J. F. Dols, and A. Sala, "Asynchronous sensor fusion of GPS, IMU and CAN-based odometry for heavy-duty vehicles," *IEEE Trans. Veh. Technol.*, vol. 70, no. 9, pp. 8617–8626, Sep. 2021.
[16] X. Wang et al., "SdoNet: Speed odometry network and noise adapter for vehicle integrated navigation," *IEEE Internet Things J.*, vol. 10, no. 21, pp. 19328–19343, Nov. 2023.
[17] W. Liu et al., "TLIO: Tight learned inertial odometry," *IEEE Robot. Autom. Lett.*, vol. 5, no. 4, pp. 5653–5660, Oct. 2020.
[18] Y. Wang, J. Kuang, X. Niu, and J. Liu, "LLIO: Lightweight learned inertial odometer," *IEEE Internet Things J.*, vol. 10, no. 3, pp. 2508–2518, Feb. 2023.
[19] B. Zhou et al., "DeepVIP: Deep learning-based vehicle indoor positioning using smartphones," *IEEE Trans. Veh. Technol.*, vol. 71, no. 12, pp. 13299–13309, Dec. 2022.
[20] T. Zhang, M. Yuan, L. Wei, Y. Wang, H. Tang, and X. Niu, "MR-ULINS: A tightly-coupled UWB-LiDAR-inertial estimator with multi-epoch outlier rejection," *IEEE Robot. Autom. Lett.*, vol. 9, no. 12, pp. 11786–11793, Dec. 2024.
[21] Y. Assayag, H. Oliveira, E. Souto, R. Barreto, and R. Pazzi, "Adaptive path loss model for BLE indoor positioning system," *IEEE Internet Things J.*, vol. 10, no. 14, pp. 12898–12907, Jul. 2023.
[22] A. A. Morgan, "On the accuracy of BLE indoor localization systems: An assessment survey," *Comput. Electr. Eng.*, vol. 118, Sep. 2024, Art. no. 109455.
[23] Y. Assayag, H. Oliveira, E. Souto, R. Barreto, and R. Pazzi, "A model-based BLE indoor positioning system using particle swarm optimization," *IEEE Sensors J.*, vol. 24, no. 5, pp. 6898–6908, Mar. 2024.
[24] T. Qin, T. Chen, Y. Chen, and Q. Su, "AVP-SLAM: Semantic visual mapping and localization for autonomous vehicles in the parking lot," in *Proc. IEEE/RSJ Int. Conf. Intell. Robots Syst. (IROS)*, Oct. 2020, pp. 5939–5945.
[25] T. Qin et al., "Crowd-sourced NeRF: Collecting data from production vehicles for 3D street view reconstruction," *IEEE Trans. Intell. Transp. Syst.*, vol. 25, no. 11, pp. 16145–16156, Nov. 2024.
[26] H. Luo, F. Zhao, M. Jiang, H. Ma, and Y. Zhang, "Constructing an indoor floor plan using crowdsourcing based on magnetic fingerprinting," *Sensors*, vol. 17, no. 11, p. 2678, Nov. 2017.
[27] A. Ayanoglu, D. M. Schneider, and B. Eitel, "Crowdsourcing-based magnetic map generation for indoor localization," in *Proc. Int. Conf. Indoor Positioning Indoor Navigat. (IPIN)*, Sep. 2018, pp. 1–8.
[28] M. Kwak, C. Hamm, S. Park, and T. T. Kwon, "Magnetic field based indoor localization system: A crowdsourcing approach," in *Proc. Int. Conf. Indoor Positioning Indoor Navigat. (IPIN)*, Sep. 2019, pp. 1–8.
[29] Y. Wang, J. Kuang, T. Liu, X. Niu, and J. Liu, "CrowdMagMap: Crowdsourcing-based magnetic map construction for shopping mall," *IEEE Internet Things J.*, vol. 11, no. 3, pp. 5362–5373, Feb. 2024.
[30] J. Kuang et al., "Smartphone built-in sensors based vehicle integrated positioning method," *J. Chin. Inertial Technol.*, vol. 28, no. 6, pp. 701–708, 2020.
[31] Y. Wang, J. Kuang, Y. Li, and X. Niu, "Magnetic field-enhanced learning-based inertial odometry for indoor pedestrian," *IEEE Trans. Instrum. Meas.*, vol. 71, pp. 1–13, 2022.
[32] K. Levenberg, "A method for the solution of certain non-linear problems in least squares," *Quart. Appl. Math.*, vol. 2, no. 2, pp. 164–168, Jul. 1944.
[33] D. W. Marquardt, "An algorithm for least-squares estimation of nonlinear parameters," *J. Soc. for Ind. Appl. Math.*, vol. 11, no. 2, pp. 431–441, Jun. 1963.
[34] Y. Li, X. Niu, P. Zhang, H. Lan, Y. Zhuang, and N. El-Sheimy, "Smartphone-based indoor navigation using PDR and magnetic matching," in *Proc. 28th Int. Tech. Meeting Satell. Division Inst. Navigat. (ION GNSS+)*, 2015, pp. 2060–2066.

Jian Kuang received the B.Eng. and Ph.D. (Hons.) degrees in geodesy and survey engineering from Wuhan University, Wuhan, China, in 2013 and 2019, respectively. He is currently an Associate Professor with the GNSS Research Center, Wuhan University. His research interests include magnetic field-based navigation, inertial navigation, pedestrian navigation, and indoor positioning.

Yan Wang received the B.Eng. degree in chemical engineering and technology and the M.S. degree in computer applied technology from China University of Mining and Technology, Xuzhou, China, in 2016 and 2019, respectively. He is currently pursuing the Ph.D. degree with the GNSS Research Center, Wuhan University, Wuhan, China. His research interests include indoor navigation, sensor fusion algorithm, and computer vision.

Longyang Ding, received the B.E. degree (Hons.) in surveying and mapping engineering and the M.S. degree (Hons.) in navigation, guidance and control from Wuhan University, Wuhan, China, in 2022 and 2025, respectively. His research interests include GNSS/INS/magnetic-field integration for smartphone-based navigation and state estimation.

Baoding Zhou (Member, IEEE) received the Ph.D. degree in photogrammetry and remote sensing from Wuhan University, Wuhan, China, in 2015. He is currently an Associate Professor with the College of Civil and Transportation Engineering, Shenzhen University, Shenzhen, China. His research interests include indoor localization and mapping, mobile computing, and intelligent transportation.

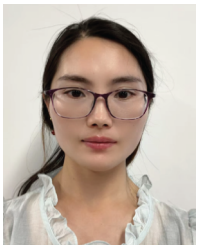

Liping Xu received the master's degree in navigation guidance and control from Southeast University in 2014. She is currently a Core Member of the GNSS Research and Development Team with Transsion Company. Her research interests include inertial navigation, satellite navigation, and integrated positioning.

Li Cao received the B.Eng. degree in electronic information engineering, Hunan Technology and Business University in 2012. He is currently the Head of WCN with Transsion. He has been deeply involved in the field of WCN for 13 years and won the Excellent Patent Award from Shenzhen Municipal Government in 2019. He has been granted over 26 patents.

Lanqin He received the master's degree in communication engineering, Chongqing University of Posts and Telecommunications in 2020. His research interests include mobile navigation and positioning at OPPO and Transsion Holdings.

Yunhui Wen received the B.Eng. degree from the Department of Surveying and Mapping Engineering, Heilongjiang Institute of Technology in 2011. Currently, he is responsible for testing and technical research related to GNSS, BT, WIFI, NFC, and telephone with Transsion.

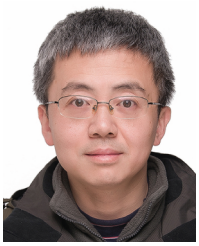

Xiaoji Niu (Member, IEEE) received the bachelor's and Ph.D. (Hons.) degrees from the Department of Precision Instruments, Tsinghua University in 2002 and 1997, respectively. He performed post-doctoral research with the University of Calgary, Canada, and worked as a Senior Scientist with SiRF Technology Inc. He is currently leading the Integrated and Intelligent Navigation (i2Nav) Group. He is a Professor with the GNSS Research Center, Wuhan University, China. His research interests focus on GNSS/INS integration, low-cost navigation sensor fusion, and relevant new applications. He has published more than 200 academic articles and owns more than 50 patents.